

Hydrate growth in granular materials: implication to hydrate bearing sediments

Tae Sup Yun*

School of Civil and Environmental Engineering, Yonsei University, Seoul 120-749, Republic of Korea

J. Carlos Santamarina

School of Civil and Environmental Engineering, Georgia Institute of Technology, Atlanta, GA

30332-0355, USA

ABSTRACT: It is often assumed that the properties of hydrate-bearing sediments are affected by hydrate growth habits in pores. We test this hypothesis by stochastically simulating hydrate growth in pore space of a simple cubic packing of mono-sized spherical sediment grains, and assume three extreme nucleation preferences in the absence of heat or mass transport limitations, and without interfacial surface tension: (1) Homogeneous nucleation produces isolated nuclei and a highly porous hydrate mass; (2) Heterogeneous nucleation results in combined surface coating and frame-building hydrate structures; and (3) Preferential heterogeneous nucleation on pre-existing hydrate surfaces leads to hydrate growth into the pore space. Spatial distribution of hydrate is analyzed to investigate the surface coating density, grain connectivity and mass density of hydrate cluster. Results show that surface coating density is predominant for heterogeneous nucleation and grain connectivity by hydrates is lower than the hydrate volume fraction in all cases. Therefore, a slow increase in stiffness is anticipated at low hydrate volume fraction. The highly porous hydrate structure formed by homogeneous nucleation and dense hydrate cluster are discussed with the relevance to the geomechanical and physical properties of hydrate-bearing sediments.

Key words: hydrate bearing sediment, nucleation, crystal growth, physical property

1. INTRODUCTION

The nucleation and subsequent growth of a solid phase within the pore space of granular materials is a common process in nature; examples include mineral dissolution and re-precipitation during soil diagenesis (Casey et al., 1993; Wagner et al., 2005), nucleation of metals on substrates (Heinemann et al., 1979; Liu et al., 2007), biological mineralization (Nancollas, 1977), ice formation in frozen grounds (Fowler and Noon, 1997), and hydrate formation in seafloor sediments and beneath the permafrost regions. In particular, the presence of hydrates within sediments inherently influences the characteristic behavior of hydrate bearing sediments, and its implication becomes critical in the context of submarine landslides (Kayen and Lee, 1991; Maslin et al., 2004), instability problems in oil production (Prassl et al., 2005), methane recovery from hydrates (Collett and Kuusk-

raa, 1998; Max and Lowrie, 1996), and possible climate effects (Hornbach et al., 2004; Kvenvolden and Rogers, 2005).

The kinetics and phase equilibrium of hydrate formation in *unbound fluid media* (e.g., free water condition without porous media) have been extensively investigated in terms of pressure, temperature, co-existing gasses, and salt contents (Kashchiev and Firoozabadi, 2002; Vysniauskas and Bishnoi, 1983). On the other hand, hydrate nucleation and growth in the *pore space of sediments* are affected by pore size and interfacial phenomena (Clennell et al., 1999; Henry et al., 1999) and are often limited by chemical and thermal transport rates (Katsuki et al., 2007; Kvamme, 2002). The nucleation and growth habit of hydrates vary depending on the hydrate formation techniques used in the laboratory and observations of natural hydrate-bearing sediments. In the laboratory, hydrate formation methods include dissolved gas method, partial water saturation method, ice-seeding method, and hydrate premixing method, while their impact on physical properties (stiffness, strength, hydraulic, thermal and electrical conductivities) changes with the size and distribution of hydrates relative to the sediment grains (see detailed discussion in Waite et al., 2009). It is anticipated that growth habit and corresponding hydrate structures can have a profound effect on sediment stiffness, strength and all types of diffusion and conduction properties; yet, hydrate formation in sediments remains poorly known in part due to experimental difficulties.

Homogenous nucleation occurs spontaneously within the fluid and away from boundaries, typically under high degrees of supersaturation. The presence of impurities, such as mineral surfaces and pre-existing hydrate, facilitates nucleation, which is referred as heterogeneous nucleation (Myerson, 2002). Nano-scale surface morphology and the atomic structure of mineral substrates determine the local electric field that facilitates heterogeneous nucleation and subsequent growth on mineral substrates, and the spatial distribution of point defects (e.g., surface roughness) is the most important factor to determine cluster size distribution and nucleation rate (Stoyanov, 1974; Vallat-Sauvain et al., 2005). The water-gas-mineral and water-hydrate-mineral contact angles cap-

*Corresponding author: taesup@yonsei.ac.kr

ture the preferential interactions between participating phases (Evans and Lane, 1972; Hirata and Mori, 1998). While further nucleation favors in the presence of already formed hydrates, nucleation (exothermic event by newly formed hydrates) and dissociation (endothermic event of pre-existing hydrates) are concurrent and opposite trends. Thus, stable crystal growth takes place only after nuclei exceed the critical size. Thereafter, the interfacial tension and the energetic advantages of continuous nucleation on the surface of pre-existing hydrates are combined to promote nuclei clustering and Ostwald ripening (Max et al., 2006; Myerson, 2002; Ng et al., 1996). The nucleation rate and growth pattern are dominated by the degree of supersaturation, chemical diffusion, temperature, latent heat of formation and heat transfer. Crystal growth in small pores is hindered by confinement and the emergence of interfacial tension between the phases (Clennell et al., 1999). In particular, the angular geometry that characterizes crystal growth in large pores changes into spherical boundaries as crystals grow across small pore throats in fine-grained soils (Adams and Gast, 1997; Everett, 1961).

In this study, we stochastically simulate various nucleation and growth habits of hydrates in granular materials to discuss their potential impacts on sediment properties such as stiffness, strength, and all forms of conduction and diffusion phenomena. Homogeneous and heterogeneous nucleations are simulated based on the simplified formation criteria.

2. METHODS

We consider mono-sized spherical sediment grains packed in a simple cubic configuration (grain diameter d , Fig. 1a). Invoking symmetry within the repetitive unit, we model the small cube size $d/2$ that contains a quarter hemisphere (Fig. 1b). This volume is divided into $N = 20 \times 20 \times 20$ with equally sized discrete voxels. A voxel at location (i, j, k) belongs to the sediment grain if the distance to the origin is $\sqrt{(i^2 + j^2 +$

$k^2) \leq N$; otherwise, it is in the pore space. The number of voxels is 4184 for grain voxels and 3806 for pore voxels. Then, the pore voxels contacted with the mineral surface are identified for simulation with the number of 498. Crystallization preferences are defined in terms of probability to simulate the three extreme hydrate growth patterns as follows.

Homogeneous nucleation is realized by assigning equal probability of nucleation to all fluid voxels in the pore space. Crystallization randomly occurs by selecting one among candidate voxels and converting it into hydrate. Isolated crystals may form without any bonds to other hydrate voxels or grain surface. Clearly, isolated crystals do not influence the small-strain mechanical characteristics of the granular skeleton but can be mobilized by fluid flow.

Heterogeneous nucleation is modeled by preferentially forming hydrates on the grain surface or on a pre-existing hydrate. The simulation starts by converting a randomly selected fluid voxel on the grain surface into hydrate. Candidate voxels for further nucleation are any fluid voxel connected to hydrate or to the grain surface. This type of hydrate growth promotes mineral surface coating (i.e., all hydrate voxels are either bonded to other hydrate voxels or to mineral surface) and prevents the formation of isolated mobile hydrate.

Heterogeneous "akin" nucleation refers herein to preferential hydrate nucleation on pre-existing hydrate. The first seed is randomly selected among fluid voxels on the grain surface. Thereafter, candidate fluid voxels for further nucleation are limited to those which are in contact with pre-formed hydrate, thus isolated hydrate voxels can not develop in this case either.

The probability of crystallization by above three nucleation criteria is plotted in Figure 2. In homogeneous nucleation, all the pore voxels are candidate at the beginning and the number of candidate voxels gradually decreases as nucleation continues. On the other hand, the number of candidate voxels slightly increases at the beginning and decreases as the volumetric fraction of hydrate V_h (the ratio between the

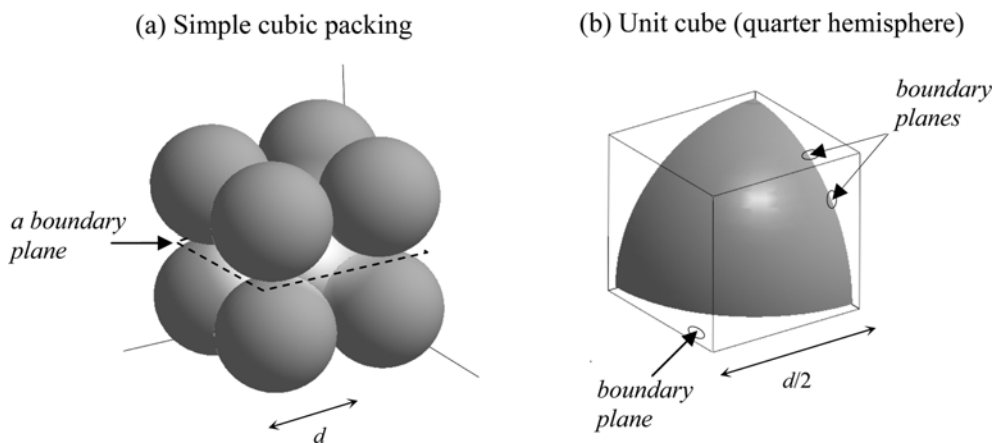


Fig. 1. Simple cubic packing of monosized particles. The simulated volume is a cube size $d/2$ that contains a quarter hemisphere. Boundary planes are tangent at inter-particle contacts.

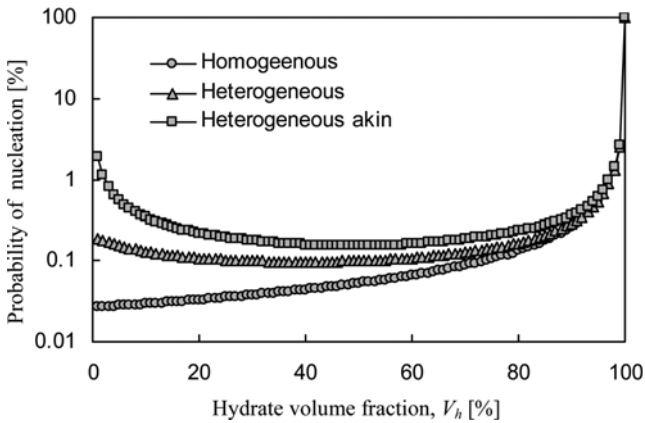


Fig. 2. Probability of hydrate formation for three nucleation criteria.

number of hydrate voxels over the total number of voxels in the pore space, N_h/N_{pore} reaches 100%. Heterogeneous akin nucleation shows similar aspect of crystallization probability whose values are higher than heterogeneous nucleation. It is attributed to the lower number of candidate voxels, defined by the nucleation criteria in this study.

Note that It is assumed that there is no interaction potential in these simulations, therefore, there is no interfacial tension; hydrate growth takes place in equilibrium and is not heat transport limited; there is no mass transport limitation, so hydrate growth continues until the hydrate volume fraction reaches $V_h = 100\%$.

Each nucleation case was 200 times simulated to gain the probabilistically acceptable results. For each nucleation case, the candidate voxels are pre-defined; all the pore voxels for homogeneous nucleation, pore voxels connected to grain surface for heterogeneous nucleation, and pore voxels surrounding the first seeding hydrate voxels for heterogeneous akin nucleation. Then, the uniform distributed pseudorandom generator (e.g., ‘rand’ function in MATLAB) sequentially selects one candidate voxels among candidates. Note that as one pore voxel is switched to the hydrate voxel as the simulation continues, the pore voxels are newly examined to update the candidate voxel groups. Each simulation stopped when the formed hydrate voxels correspond to the pre-defined hydrate fraction in pore space (i.e., 381 hydrate voxels are iteratively created among total 3806 pore voxels to make $V_h \sim 10\%$). Results are analyzed at pre-selected hydrate volume fractions V_h (every 1% V_h increment up to $V_h = 100\%$) to identify formation patterns, to measure the number of bonded hydrate that fills boundary planes across the pore (Fig. 1), and to evaluate the hydrate density.

3. SIMULATION RESULTS

3.1. Formation Pattern

Figure 3 shows the spatial distribution of hydrate in the

three nucleation cases and for various volume fractions V_h . Dots indicate hydrate voxels in pore space. For homogeneous nucleation, hydrate voxels connected from the grain surface and non-connected ones are independently shown. At low volume fractions V_h , most hydrate voxels in homogeneous nucleation have very low connectivity among each other and the probability of finding a hydrate voxel on the grain surface is approximately close to $V_h \cdot N_{grain_surface} / N_{pores}$ ($N_{grain_surface} = 498$, $N_{pores} = 3806$). As the hydrate volume fraction V_h increases, a weakly connected cluster develops on the surface and in the pore space and becomes interconnected to form highly porous structure (connected case shown in Fig. 3a). The highly porous network links the particle to boundary plane and isolated hydrate voxels begin diminishing once V_h reaches $\sim 40\%$ (non-connected case in Fig. 3a).

Heterogeneous nucleation exhibits a pronounced tendency to coat the grain surface. Surface coating renders an increase in inter-particle contact area; “contact enlargement” implies the early increase in skeletal stiffness of granular materials during heterogeneous nucleation (Priest et al., 2005).

Heterogeneous akin nucleation favors hydrate growth from the first seed on the grain surface into the pore. When hydrate growth reaches boundary planes, the hydrate mass has formed a structural element or truss between grains across the pore (due to the assumed cell symmetry). This type of “frame-building” hydrate growth adds stiffness and stability to the granular skeleton.

3.2. Surface Coating

“Surface coating density”, S_h is defined as the ratio of the number of hydrate voxels on the grain surface to the total number of voxels on the grain surface (e.g., $N_{grain_surface} = 481$ in this study). Figure 4a (left) presents the mean value of surface coating density S_h for 200 simulations. The early increase in S_h as a function of V_h in heterogeneous nucleation confirms its tendency towards early grain surface coating. On the other hand, while akin nucleation is seeded on the mineral surface (early increase in S_h), further growth takes place towards the pore space with slowing down surface coating trends. Homogeneous nucleation follows the theoretically predicted linear trend $S_h \approx V_h$. The variability of surface coating density is assessed in terms of the coefficient of variation cov defined as the ratio between the standard deviation s and the mean m , based on 200 simulation results. Higher variability defined based on the surface coating density implies that hydrate formation could take place any possible candidate places (e.g., grain surface without involving adjacent grain, pore space, inter-particle contact). Results in Figure 4a (right) show that variability is highest at low hydrate concentration for all the cases, i.e., when there is a maximum number of candidate voxels for nucleation. Similarly, heterogeneous nucleation displays the lowest value of cov among the three growth habits because

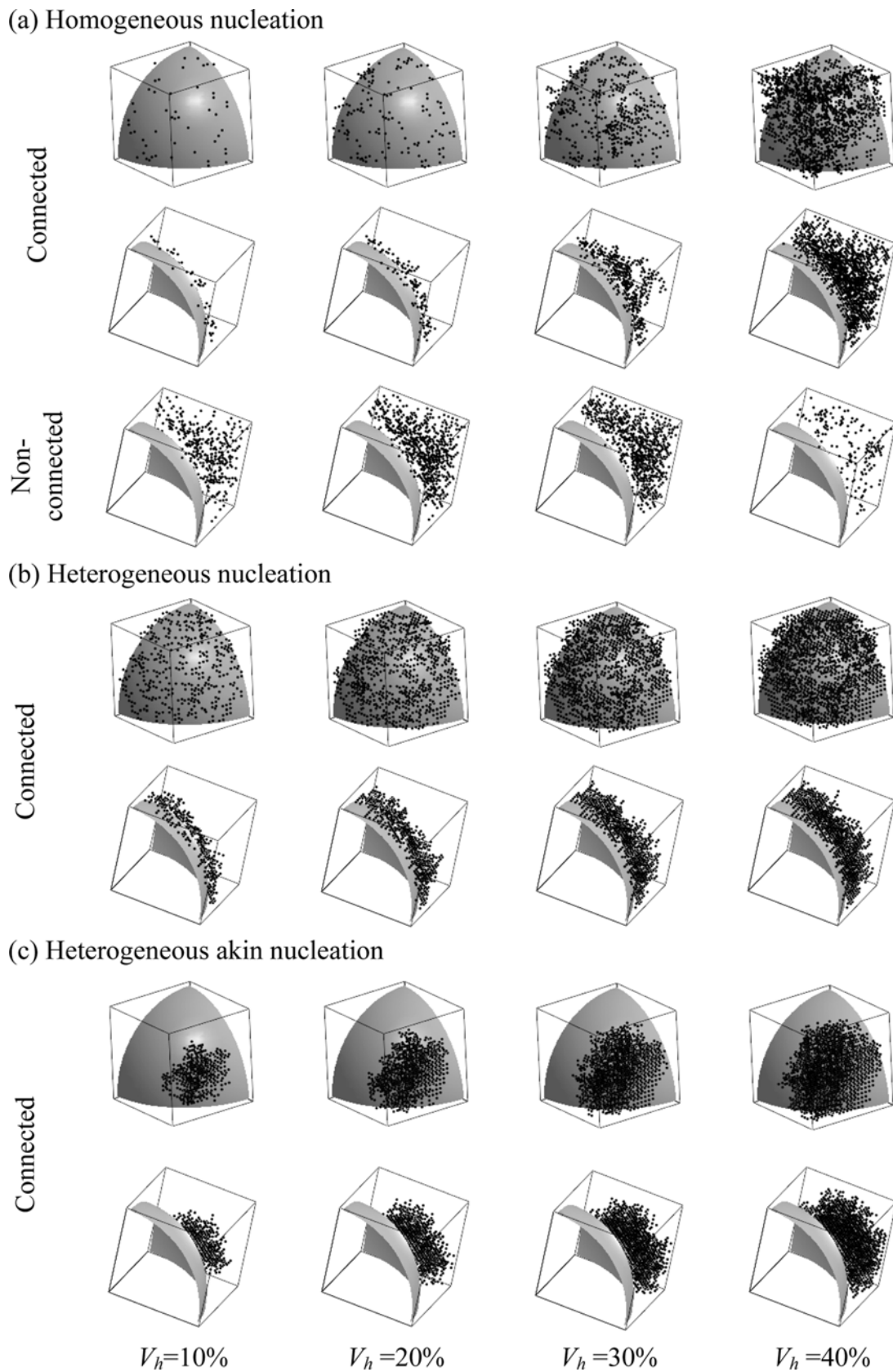


Fig. 3. Spatial distribution of hydrate voxels. Realizations at selected hydrate volume fraction V_h for three nucleation cases. Connected hydrate voxels well develop and non-connected hydrates diminish with V_h for homogeneous nucleation. All hydrate voxels in the two heterogeneous nucleation cases are connected to the particle through percolating hydrate chains.

candidate voxels are initially restricted to those on grain surfaces while the heterogeneous akin nucleation indicates the highest value of cov .

3.3. Grain Connectivity by Hydrate Phase across the Pore

Hydrate voxels gradually occur on the three boundary planes that bisect the pore space. The normalized area, A_h is defined as the ratio between the number of bonded hydrate voxels on the three boundary planes to the total number of boundary voxels, $3N \cdot (N-1) + 1 = 1141$ in this study. Isolated hydrate voxels found in homogeneous nucleation are not counted because they do not contribute to frame-building. Results are shown in Figure 4b:

- The normalized area A_h increases at a lower rate than the hydrate volume fraction V_h in the three nucleation preferences. The delayed increase in A_h is most pronounced for homogeneous nucleation until V_h 30 to 40%; further nucleation leads to a sudden increase in grain connectivity, changing isolated voxels into bonded hydrates (see Fig. 3a).

- Heterogeneous akin nucleation exhibits higher normalized area A_h than heterogeneous nucleation because the hydrate growth takes place preferentially into the pore rather than in surface coating mode.

- The coefficient of variation cov is highest at low hydrate

volume fraction (for heterogeneous akin nucleation) due to the higher degrees of freedom at the beginning of the process when V_h is low.

3.4. Hydrate Density

The strength of a solid is inversely proportional to its internal porosity. In this simulation, internal porosity within the hydrate mass implies hydrate bodies that are in contact with fluid (e.g., pore space). Therefore, we use hydrate coordination as a surrogate for porosity, where the coordination number cn of a hydrate voxel is the number of hydrate voxels that are in direct face contact with either the mineral grain or other hydrate voxels. It varies from $cn = 0$ for an isolated hydrate voxel, to $cn = 6$ for a hydrate voxel that is fully surrounded by either hydrate or mineral. Histograms of coordination numbers at different hydrate volume fractions V_h are presented in Figure 5 for the three nucleation preferences. In all cases, the coordination number increases as the hydrate concentration increases, and eventually reaches $cn = 6$ at $V_h = 1$.

There are important differences among growth preferences, in particular: (1) the high coordination number has highest frequency in heterogeneous akin nucleation (e.g., hydrate structure is least porous), and (2) the relatively

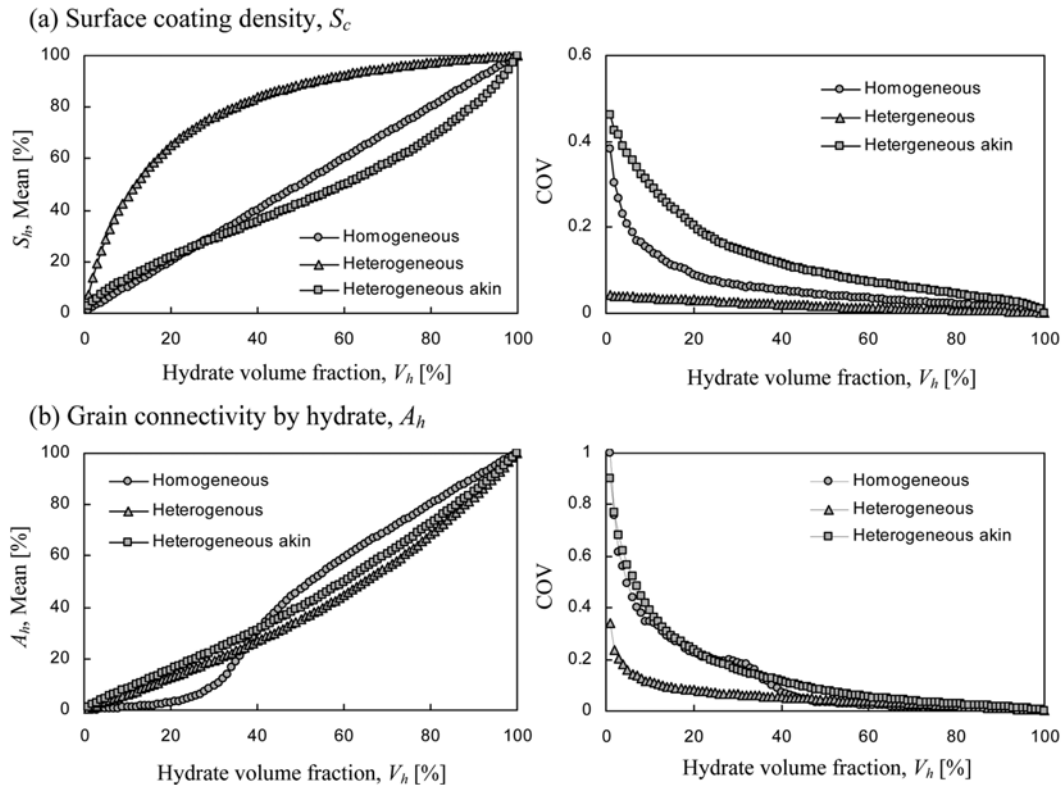


Fig. 4. Statistical evaluation of growth patterns as a function of hydrate volume fraction V_h - Results for the three nucleation cases. (a) Surface coating density S_c . (b) Hydrate at boundary planes. Mean and coefficient of variation are computed using 200 simulations for each nucleation preference.

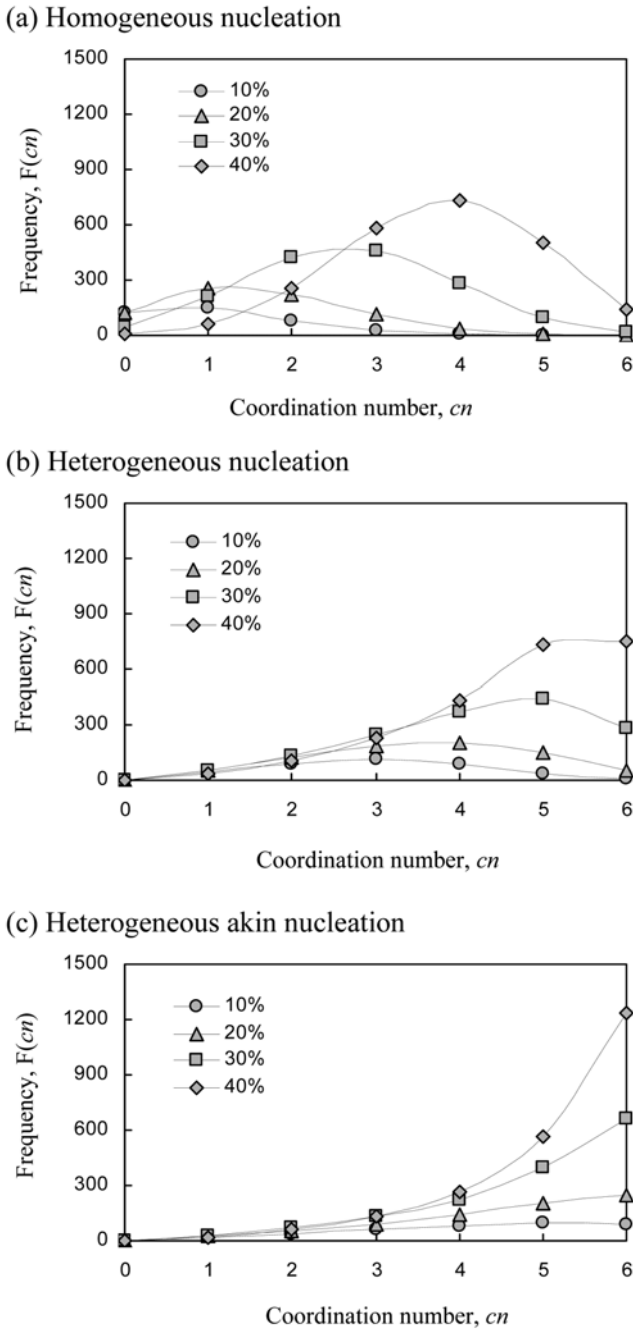


Fig. 5. Histogram of coordination number cn for each nucleation preference at different volume fractions V_h . The coordination number varies between $cn = 0$ for a hydrate voxel surrounded by pore space, to $cn = 6$ for a hydrate voxel surrounded by adjacent hydrate or grain surface.

lower coordination numbers prevail in homogeneous nucleation (e.g., hydrate structure is most porous and the internal porosity is highest) compared with others. These observations are in agreement with geometric features observed in Figure 3 and complement connectivity trends noted in Figure 4.

The hydrate mass density is further analyzed based on the porous hydrate structure. Once hydrate voxels are created

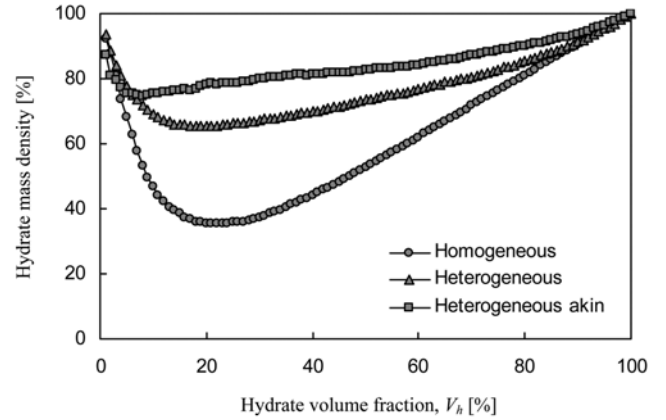


Fig. 6. Hydrate mass density versus hydrate volume fraction V_h . Mass density is computed with the number of hydrate voxels normalized by the bulk unit volume of hydrate cluster. Homogeneous nucleation shows the lowest mass density, implying highly porous structure.

for a given hydrate volume fraction and nucleation criteria, the imaginary unit volume of a single hydrate mass is obtained by connecting circumferential hydrate voxels and computing the volume of enclosed space. That is, the unit volume of hydrate mass represents the imaginary non-porous and solid hydrate within which the original and porous hydrate voxels reside. Then, the number of hydrate voxels is normalized by the unit volume to gain the hydrate mass density (Fig. 6). Heterogeneous akin nucleation shows the densest structure than other nucleation cases (e.g., less porous structure), while the mass density of homogeneous nucleation indicates the lowest values with the hydrate volume fraction (e.g., more porous structure). This observation coincides with the results of coordination number.

4. DISCUSSION – IMPLICATION TO HYDRATE-BEARING SEDIMENTS

Hydrate formation can (1) increase the effective inter-particle contact area when it nucleates near grain contacts, and (2) increase the stability of the granular skeleton when it adds trusses between grains across the pore space, i.e., “frame-building” (note that this effect is captured by grain connectivity by hydrate in Fig. 4b). Hydrates formed in pore space without involving surrounding particles may not be contributory to the geomechanical properties of bulk hydrate-bearing sediments.

The small-strain stiffness of granular materials is determined by the number and deformability of inter-particle contacts. Hertzian contact theory models that the small-strain stiffness of the granular skeleton E_{skel} is proportional to the square root of the inter-particle contact area A

$$E_{skel} = \sqrt{\frac{A}{\pi R}} \cdot \frac{G_g}{(1 - \nu_g)} \quad (1)$$

where G_g and n_g are shear stiffness and Poisson ratio of the mineral that makes the grains and R is the radius of a grain. Hydrate formation results in the increase of initial inter-particle contact area to $A' = (r_c + r_h)^2 \pi$ where r_c is the inter-particle contact radius and r_h is the increase radius by formed hydrate on the given cross-sectional area. Then, A' is directly related to the grain connectivity A_h defined in this study as $A' \approx r_c^2 \pi + A_h$. Results gathered with three crystallization preferences show that the probability of finding hydrate on the planes of contacts is lower than the hydrate volume fraction V_h , particularly at low V_h values (Fig. 4b). In summary, a slow increase in stiffness is expected at low hydrate concentration V_h because 1) $E_{skel} \propto \sqrt{A}$, 2) Probability of hydrate formation at contacts $\leq V_h$, particularly at low V_h , and 3) the high coefficient of variation in A_h at low V_h . Experimental observations in the laboratory (Kunerth et al., 2000; Yun et al., 2005) and field evidence (Helgerud et al., 1999; Kleinberg et al., 2003; Lee and Collett, 2001) are in agreement with these predictions when hydrate forms from dissolved gas. In contrast, when hydrate formation occurs in unsaturated sediments, water migrates to inter-particle contacts, hydrate forms at contacts and causes a very high increase in stiffness at low V_h values (unsaturated method, Priest et al., 2005).

The large-strain mechanical behavior of granular materials involves particle-level processes that are affected by the type of hydrate nucleation. The three hydrate growth patterns increase the solid fraction and the tendency to volume dilation during shear combined with rotational frustration (see data in Ebinuma et al., 2005; Masui et al., 2005). Even small amount of hydrates formed at inter-particle contacts (e.g., heterogeneous and heterogeneous akin nucleation) cements particles together and substantially increases the strength and stiffness. On the other hand, pore-filling hydrates (e.g., homogeneous nucleation) begin playing a critical role on the geomechanical properties when $V_h > 30\sim 40\%$ (Yun et al., 2007). Furthermore, it is reported that the cohesion and dilation angle increase with increasing hydrate volume fraction while friction angle is mostly independent of hydrate volume fraction (Waite et al., 2009).

Thermal conductivity values for sediment components rank as follows: $k_{\text{gas}} < k_{\text{hydrate}} < k_{\text{water}} < k_{\text{mineral}}$. Therefore, the thermal conduction in sediments takes place primarily through inter-particle contacts and it is enhanced by high inter-particle coordination and by the presence of water (Yun and Santamarina, 2008). It is anticipated that nominal changes in thermal conductivity would occur due to hydrate formation, regardless of the growth preference because the thermal conductivity of hydrates is close to that of water. However, the previous experimental results show that the sediments has higher thermal conductivity upon hydrate formation presumably due to the cryogenic suction and hydrate segregation, improved contact quality, and the reduction in interfacial thermal resistance when the grain-

liquid interface changes to the grain-hydrate (Cortes et al., 2009). Although different hydrate nucleation and growth habits determine unique microstructure of hydrates, the effect would not be significant on the bulk thermal conductivity in hydrate-bearing sediments at the macro-scale as long as the sediment remains water saturated. The formation of secondary phase in pore space for surface coating and pore filling cases uniquely determines the thermal conductivity of bulk granular materials (Yun and Evans, 2010). Yet, the heat transfer would be facilitated through less porous hydrate structure that grows in the pore space and connects grains due to the lower thermal resistance between phases at the particle-scale.

Fluid flow in granular materials is determined by pore size and shape and the presence of solid scatters which cause momentum loss (e.g., Kozeny-Carman equation; Ma and Ruth, 1994; numerical simulations in Gao and Sharma, 1994; Rothman, 1988). The pore space can be also categorized into the network of pore chambers (e.g., large pore space enclosed by grains) and pore channels that inter-connect the pore chambers (Abichou et al., 2004; Al-Raoush and Willson, 2005). The web of pore chambers and pore channels determines the behavior of fluid flow and the connectivity among pore chambers affects the hydraulic conductivity in porous media. The nucleation patterns thus influence on both tortuosity and size of pore channel and interconnectivity (Hagen-Poiseuille equation that has been widely used for hydraulic network model informs that the flow rate is related to the quartic r^4 where r is the equivalent radius of pore channel). Thus, homogeneous nucleation tends to decrease permeability more significantly than heterogeneous nucleation (Liu and Flemings, 2006) and estimates values turn out to be close to in-situ permeability values (Kleinberg et al., 2003). Yet, heterogeneous and heterogeneous akin nucleation may block pore channel and throat and cause a pronounced decrease in permeability even at low values of V_h .

Note that the nucleation and growth pattern are complicated process rather than dominated by a single criteria. Growth of hydrates changes spatial distribution of pore space so that locations where the free energy is minimized accordingly change. Furthermore, crystallization involving mass transport and heat exchange newly defines available resources, which is not encountered in this study. However, the stochastic simulation provides the first approximation of crystallization pattern of hydrates in pore space with relevance to physical behaviors of hydrate-bearing sediments.

5. CONCLUSIONS

Numerical simulation results show that hydrate growth preferences (in equilibrium and in the absence of surface tension) lead to distinct spatial distributions of hydrate in the pore space. Hydrate habit in the pore space is combined

with pore- and particle-scale physical processes to determine the macro-scale properties of hydrate bearing sediments:

- Homogeneous nucleation, which may unlikely occur in sediments, produces isolated and highly porous hydrate structure. Hydrate mass density tends to increase at hydrate volume fraction $V_h = 20\sim 30\%$, yet stilling showing most porous network compared with heterogeneous and heterogeneous akin nucleation. Preferential coating of grain surface and frame-building by hydrates create hydrate mass with high density by connecting neighboring particles. Spatial distribution of hydrates in pore space by given crystallization pattern entails the unique evolution in grain connectivity, which in turn affects the geomechanical and physical properties of hydrate bearing sediments.

- The observation that the grain connectivity by hydrate is lower than the hydrate volume fraction coincides with the laboratory and in-situ investigation to evaluate the geomechanical behaviors of hydrate-bearing sediments.

- Evaluation of physical properties needs enormous efforts not only for the scientific understanding of behaviors of hydrate-bearing sediments but also for the engineering application (e.g., production, stability), while limited access to the natural hydrate system and difficulties of synthetic hydrates in the laboratory hamper the further investigation. While simulation results is not directly correlated with the conduction phenomena (e.g., thermal, hydraulic and electrical conduction) in this study, the stochastic modeling of hydrate nucleation and growth hints the understanding of approximated conduction properties of hydrate-bearing sediments.

- The investigation of evolutionary microstructure attributed to the hydrate formation presented in this study focuses on the particle-scale. Although the grain connectivity by hydrate growth in pore space and internal porosity of hydrates should significantly influence on the particle-scale phenomena, the up-scaling to the bulk scale requires a caution to assess the relevance of nucleation habit to the macro-scale manifestation.

ACKNOWLEDGMENTS: Support for this study was provided by U.S. Department of Energy, the Goizueta Foundation, and Yonsei University Research Fund of 2009. Special thanks to D.H. Kang during revision process.

REFERENCES

- Abichou, T., Benson, C.H., and Edil, T.B., 2004, Network model for hydraulic conductivity of sand-bentonite mixtures. *Canadian Geotechnical Journal*, 41, 698–712.
- Adams, A.W. and Gast, A.P., 1997, *Physical chemistry of surfaces*. John Wiley and Sons, New York, 784 p.
- Al-Raoush, R.I. and Willson, C.S., 2005, Extraction of physically realistic pore network properties from three-dimensional synchrotron X-ray microtomography images of unconsolidated porous media systems. *Journal of Hydrology*, 300, 44–64.
- Casey, W.H., Westrich, H.R., Banfield, J.F., Ferruzzi, G., and Arnolds, G.W., 1993, Leaching and reconstruction at the surfaces of dissolving chain-silicate minerals. *Nature*, 366, 253–255.
- Clennell, M.B., Hovland, M., Booth, J.S., Henry, P., and Winters, W.J., 1999, Formation of natural gas hydrates in marine sediments 1. Conceptual model of gas hydrate growth conditioned by host sediment properties. *Journal of Geophysical Research*, 104, 22985–23003.
- Collett, T.S. and Kuuskraa, V.A., 1998, Emerging U.S. gas resources – 4. Hydrates contain vast store of world gas resources. *Oil and Gas Journal*, 96, 90–95.
- Cortes, D., Martin, A., Yun, T.S., Francisca, F.M., Santamarina, J.C., and Ruppel, C., 2009, Thermal conductivity of hydrate bearing sediments. *Journal of Geophysical Research*, 114, B11103.
- Ebinuma, T., Kamata, Y., Minagawa, H., Ohnuma, R., Nagao, J., and Narita, H., 2005, Mechanical properties of sandy sediment containing methane hydrate. In: *Proceedings of the 5th International Conference on Gas Hydrate*, Trondheim, June 13–16, 3, p. 958–961.
- Evans, L.F. and Lane, J.E., 1972, Line tension and ice nucleation theory. *Journal of the atmospheric sciences*, 30, 326–331.
- Everett, D.H., 1961, The thermodynamics of frost damage to porous solids. *Transactions of the Faraday Society*, 57, 1541–1551.
- Fowler, A.C. and Noon, C.G., 1997, Formation of massive ice in permafrost. Lulea, Sweden, 81.
- Gao, Y. and Sharma, M., 1994, A LGA model for dispersion in heterogeneous porous media. *Transport in porous media*, 17, 19–32.
- Heinemann, K., Kim, H.K., and Poppa, H., 1979, Nucleation, growth, and postdeposition thermally induced epitaxy of gold on sapphire. *Journal of Vacuum Science and Technology*, 16, 622–624.
- Helgerud, M.B., Dvorkin, J., Nur, A., Sakai, A., and Collett, T., 1999, Elastic-wave velocity in marine sediments with gas hydrates: effective medium modeling. *Geophysical Research Letters*, 26, 2021–2024.
- Henry, P., Thomas, M., and Clennell, M.B., 1999, Formation of natural gas hydrates in marine sediments 2. Thermodynamic calculations of stability conditions in porous sediments. *Journal of Geophysical Research*, 104, 23005–23022.
- Hirata, A. and Mori, Y.H., 1998, How liquids wet clathrate hydrates: Some macroscopic observations. *Chemical Engineering Science*, 53, 2641–2643.
- Hornbach, M.J., Saffer, D.M., and Holbrook, W.S., 2004, Critically pressured free-gas reservoirs below gas-hydrate provinces. *Nature*, 427, 142–144.
- Kashchiev, D. and Firoozabadi, A., 2002, Nucleation of gas hydrates. *Journal of Crystal Growth*, 243, 476–489.
- Katsuki, D., Ohmura, R., Ebinuma, T., and Narita, H., 2007, Methane hydrate crystal growth in a porous medium filled with methane-saturated liquid water. *Philosophical Magazine*, 87, 1057–1069.
- Kayen, R.E. and Lee, H.J., 1991, Pleistocene slope instability of gas hydrate-laden sediment on the Beaufort sea margin. *Marine Geotechnology*, 10, 125–141.
- Kleinberg, R.L., Flaum, C., Griffin, D.D., Brewer, P.G., Malby, G.E., Peltzer, E.T., and Yesinowski, J.P., 2003, Deep sea NMR: Methane hydrate growth habit in porous media and its relationship to hydraulic permeability, deposit accumulation, and submarine slope stability. *Journal of Geophysical Research*, 108, 2508.
- Kunrath, D.C., Weinberg, D.M., Rector, J.W., Scott, C.L., and Johnson, J.T., 2000, Acoustic laboratory measurements during the formation of a THF-hydrate in unconsolidated porous media. *Journal of seismic exploration*, 9, 337–354.

- Kvamme, B., 2002, Kinetics of hydrate formation from nucleation theory. *International Journal of Offshore and Polar Engineering*, 12, 256–263.
- Kvenvolden, K.A. and Rogers, B.W., 2005, Gaia's breath - Global methane exhalations. *Marine and Petroleum Geology*, 22, 579–590.
- Lee, M.W. and Collett, T.S., 2001, Elastic properties of gas hydrate-bearing sediments. *Geophysics*, 66, 763–771.
- Liu, X. and Flemings, P.B., 2006, Passing gas through the hydrate stability zone at southern hydrate ridge, offshore Oregon. *Earth Planetary Science Letters*, 241, 211–226.
- Liu, Y., Overzet, L., and Goeckner, M., 2007, Effect of substrate on the nucleation and growth of aluminum films deposited from methylpyrrolidine alane. *Thin Solid Films*, 515, 6730–6736.
- Ma, H. and Ruth, D.W., 1994, A numerical analysis of the interfacial drag force for fluid flow in porous media. *Transport in porous media*, 17, 87–103.
- Maslin, M., Owen, M., Day, S., and Long, D., 2004, Linking continental-slope failures and climate change: Testing the clathrate gun hypothesis. *Geology*, 32, 53–56.
- Masui, A., Haneda, H., Ogata, Y., and Aoki, K., 2005, The effect of saturation degree of methane hydrate on the shear strength of synthetic methane hydrate sediments. In: *Proceedings of the 5th International Conference on Gas Hydrates*, Trondheim, June 13–16, 2, p. 657–663.
- Max, M.D. and Lowrie, A., 1996, Oceanic methane hydrates: a 'frontier' gas resource. *Journal of Petroleum Geology*, 19, 41–56.
- Max, M.D., Johnson, A.H., and Dillon, W.P., 2006, *Economic geology of natural gas hydrate*. Springer, Dordrecht, 341 p.
- Myerson, A.S., 2002, *Handbook of industrial crystallization*. Butterworth-Heinemann, Boston, 313 p.
- Nancollas, G.H., 1977, The mechanism of biological mineralization. *Journal of Crystal Growth*, 42, 185–193.
- Ng, J.D., Lorber, B., Witz, J., Theobald-Dietrich, A., Kern, D., and Giege, R., 1996, Crystallization of biological macromolecules from precipitates: Evidence of Ostwald ripening. *Journal of Crystal Growth*, 168, 50–62.
- Prassl, W.F., Peden, J.M., and Wong, K.W., 2005, A process-knowledge management approach for assessment and mitigation of drilling risks. *Journal of Petroleum Science and Engineering*, 49, 142–161.
- Priest, J.A., Best, A.I., and Clayton, C.R.I., 2005, A laboratory investigation into the seismic velocities of methane gas hydrate-bearing sand. *Journal of Geophysical Research*, 110, B04102.
- Rothman, D.H., 1988, Cellular-automation fluids: A model for flow in porous media. *Geophysics*, 53, 509–518.
- Stoyanov, S., 1974, Nucleation on point defects. *Journal of Crystal Growth*, 24–25, 293–297.
- Vallat-Sauvain, E., Bailat, J., Meier, J., Niquille, X., Kroll, U., and Shah, A., 2005, Influence of the substrate's surface morphology and chemical nature on the nucleation and growth of microcrystalline silicon. *Thin Solid Films*, 485, 77–81.
- Vysniauskas, A. and Bishnoi, P.R., 1983, Kinetic study of methane hydrate formation. *Chemical Engineering Science*, 38, 1061–1072.
- Wagner, R., Kuhn, M., Meyn, V., Pape, H., Vath, U., and Clauser, C., 2005, Numerical simulation of pore space clogging in geothermal reservoirs by precipitation of anhydrite. *International Journal of Rock Mechanics and Mining Sciences*, 42, 1070–1081.
- Waite, W.F., Santamarina, J.C., Cortes, D.D., Dugan, B., Espinoza, D.N., Germaine, J., Jang, J., Jung, J.W., Kneafsey, T.J., Shin, H., Soga, K., Winters, W.J., and Yun, T.S., 2009, Physical properties of hydrate bearing sediments. *Reviews of Geophysics*, 47, RG4003.
- Yun, T.S., Francisca, F.M., Santamarina, J.C., and Ruppel, C., 2005, Compressional and shear wave velocities in uncemented sediment containing gas hydrate. *Geophysical Research Letters*, 32, 10609.
- Yun, T.S., Santamarina, J.C., and Ruppel, C., 2007, Mechanical properties of sand, silt, and clay containing tetrahydrofuran hydrate. *Journal of Geophysical Research*, 112, B04106.
- Yun, T.S. and Santamarina, J.C., 2008, Fundamental study of thermal conduction in dry soils. *Granular Matter*, 10, 197–207.
- Yun, T.S. and Evans, T.M., 2010, Three-dimensional random network model for thermal conductivity in particulate materials. *Computers and Geotechnics*, 37, 991–998.

Manuscript received February 11, 2010

Manuscript accepted July 2, 2011